

**INVESTIGATION OF STRAIN RATE EFFECTS  
ON THE DYNAMIC RESPONSE OF A GLASS/EPOXY  
COMPOSITE PLATE UNDER BLAST LOADING BY USING  
THE FINITE-DIFFERENCE METHOD**

**M. M. Shokrieh\* and A. Karamnejad**

**Keywords:** *dynamic response, finite-difference method, progressive damage model, strain rate*

*Nonlinear equations of motion for a laminated composite plate under blast loading, based on the first-order shear deformation theory, are derived. The governing equations are solved by the finite-difference method in conjunction with the Newmark time integration scheme. The rules of material property degradation are modified to allow for strain rate effects. A progressive damage model is developed based on the modified rules of material property degradation and Hashin-type failure criteria to predict different failure modes. The validity of the method is demonstrated by quantitative and qualitative comparisons of present results with those available in the literature. Results for clamped glass/epoxy laminated composite plates with constant and strain-rate-dependent mechanical properties under a blast load are presented and compared for various ply stacking sequences, and pertinent conclusions are outlined.*

## **1. Introduction**

Due to their appropriate high energy absorption capacity, composite materials have extensive applications in structures subjected to high-intensity dynamic loads and rapid deformations. Under dynamic loads, such as blasts, the structures experience medium and high strain rates. Since mechanical properties can vary with strain rate, the dynamic response of the structures depends on the strain rate. In addition to strain rate effects, the geometrical nonlinearity due to large deformations and transverse shear strains is also an important factor in a structural analysis in such conditions.

---

Composites Research Laboratory, Center of Excellence in Experimental Solid Mechanics and Dynamics, School of Mechanical Engineering, Iran University of Science and Technology, Tehran, 16846-13114, Iran

\*Corresponding author; tel.: +98-21-7724-0540 to 50 (Ext. 2914); fax: +98-21-7749-1206; e-mail: shokrieh@iust.ac.ir

---

Russian translation published in *Mekhanika Kompozitnykh Materialov*, Vol. 50, No. 3, pp. 419-440, May-June, 2014. Original article submitted March 12, 2010; revision submitted October 9, 2013.

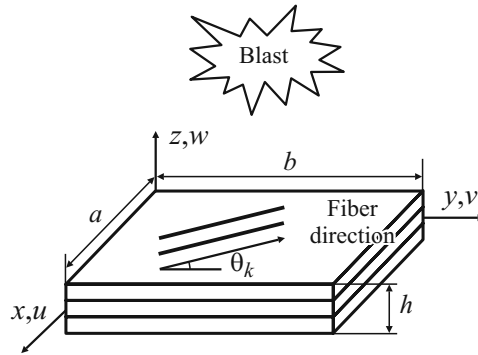


Fig. 1. Laminated composite plate under a blast load.

Composite structures under blast loads have been studied experimentally, analytically, and numerically by various researchers. Reddy [1] examined the transient response of laminated composite panels by using the finite-element method, which allows for geometrical nonlinearities. Librescu and Nosier [2] investigated the response of laminated composite flat panels to sonic boom and explosive blast loads by employing the technique of integral transforms. The transverse shear deformations, the transverse normal stresses, and higher-order effects are taken into consideration in their analysis. Turkmen and Mecitoglu [3] studied the dynamic response of a stiffened laminated composite plate subjected to blast loads experimentally and numerically. Turkmen [4] presented theoretical and experimental investigations into the dynamic response of cylindrically curved laminated composite shells subjected to blast loading by using the Galerkin and Runge–Kutta–Verner methods. Utilizing the Galerkin and finite-difference methods, Kazanci and Mecitoglu [5] studied the nonlinear dynamic response of a laminated composite plate subjected to blast loads. Chenetal [6] presented a semi-analytical finite-strip method for an analysis of the geometrically nonlinear response of rectangular composite laminated plates to dynamic loading.

But none of the above-mentioned studies consider the effects of strain rate. Batra and Hassan [7] developed a mathematical model for analyzing the transient response of a composite plate subjected to underwater blast loads. They considered strain rate effects on the transverse and shear stiffnesses. Zhu et al. [8] presented a micromechanics model taking into account the transverse shear stress, the strain rate, and inelasticity to analyze the transient response of a laminated composite plate.

In the present work, the response of a laminated composite plate under blast loading is investigated. In the macro-mechanical approach, the finite-difference method and a progressive damage modeling algorithm considering the geometric nonlinearity are used. The effects of transverse shear strain and strain rate are studied. Coupled nonlinear equations of motion for a laminated plate based on the first-order shear deformation theory (FSDT) are derived and reduced to nonlinear ordinary differential equations in the time domain by using finite-difference approximations for displacements. The Newmark time integration scheme in association with the Newton–Raphson iteration method is employed to solve the system of nonlinear equations. The mechanical properties are updated based on the values of calculated strain rate at each material point. Furthermore, the degradation of mechanical properties due to failure is considered using the rules of sudden degradation of material properties and Hashin-type failure criteria for composite materials. The damage evolution and the strain-rate-dependence of longitudinal, transverse and shear mechanical properties can be considered by the model. Moreover, the present macromechanical model is less complex than micromechanics models.

## 2. Governing Equations

Figure 1 shows a rectangular laminated composite plate subjected to a blast load. The displacement field, according to the first-order shear deformation theory, can be expressed as [9]

$$u(x, y, z, t) = u_0(x, y, t) + z\varphi_x(x, y, z),$$

$$v(x, y, z, t) = v_0(x, y, t) + z\varphi_y(x, y, z),$$

$$w(x, y, z, t) = w_0(x, y, t),$$

where  $u$ ,  $v$ , and  $w$  are displacements in the  $x$ ,  $y$ , and  $z$  directions, respectively;  $u_0$ ,  $v_0$ , and  $w_0$  denote displacements on the plane  $z = 0$ ;  $\varphi_x$  and  $\varphi_y$  are rotations of the transverse normal about the  $x$  and  $y$  axes, respectively.

The nonlinear strain–displacement relations based on the von Karman theory of plates can be written as

$$\begin{Bmatrix} \varepsilon_{xx} \\ \varepsilon_{yy} \\ \gamma_{xy} \\ \gamma_{xz} \\ \gamma_{yz} \end{Bmatrix} = \begin{Bmatrix} \varepsilon_{xx}^0 \\ \varepsilon_{yy}^0 \\ \gamma_{xy}^0 \\ \gamma_{xz}^0 \\ \gamma_{yz}^0 \end{Bmatrix} + z \begin{Bmatrix} \kappa_{xx} \\ \kappa_{yy} \\ \kappa_{xy} \\ \kappa_{xz} \\ \kappa_{yz} \end{Bmatrix} = \begin{Bmatrix} u_{0,x} + \frac{1}{2}w_{0,x}^2 \\ v_{0,y} + \frac{1}{2}w_{0,y}^2 \\ u_{0,y} + v_{0,x} + w_{0,x}w_{0,y} \\ w_{0,x} + \varphi_x \\ w_{0,y} + \varphi_y \end{Bmatrix} + z \begin{Bmatrix} \varphi_{x,x} \\ \varphi_{y,y} \\ \varphi_{x,y} + \varphi_{y,x} \\ 0 \\ 0 \end{Bmatrix}, \quad (1)$$

where,  $\varepsilon_{xx}^0$ ,  $\varepsilon_{yy}^0$ ,  $\gamma_{xy}^0$ ,  $\gamma_{xz}^0$ , and  $\gamma_{yz}^0$  are the membrane strains;  $\kappa_{xx}$ ,  $\kappa_{yy}$ ,  $\kappa_{xy}$ ,  $\kappa_{xz}$ , and  $\kappa_{yz}$  are the flexural strains or curvatures, but  $\varepsilon_{zz}$  is obviously equal to zero;  $z$  is the distance of an arbitrary point from the reference surface. The stress–strain relations for a  $k$ th layer are

$$\begin{Bmatrix} \sigma_{xx} \\ \sigma_{yy} \\ \sigma_{yz} \\ \sigma_{zx} \\ \sigma_{xy} \end{Bmatrix}^{(k)} = \begin{bmatrix} \bar{Q}_{11} & \bar{Q}_{12} & 0 & 0 & \bar{Q}_{16} \\ \bar{Q}_{12} & \bar{Q}_{22} & 0 & 0 & \bar{Q}_{26} \\ 0 & 0 & 2\bar{Q}_{44} & 2\bar{Q}_{45} & 0 \\ 0 & 0 & 2\bar{Q}_{45} & 2\bar{Q}_{55} & 0 \\ \bar{Q}_{16} & \bar{Q}_{26} & 0 & 0 & 2\bar{Q}_{66} \end{bmatrix} \begin{Bmatrix} \varepsilon_{xx} \\ \varepsilon_{yy} \\ \varepsilon_{yz} \\ \varepsilon_{zx} \\ \varepsilon_{xy} \end{Bmatrix}^{(k)}, \quad (2)$$

where  $\bar{Q}_{ij}^{(k)}$  at  $i, j = 1, 2, 6$  are the inplane reduced stiffness coefficients and  $i, j = 4, 5$  denote the through-the-thickness shear stiffness coefficients;  $\varepsilon_{yz}$ ,  $\varepsilon_{zx}$ , and  $\varepsilon_{xy}$  represent the tensorial shear strains, which are half of the engineering shear strains  $\gamma_{yz}$ ,  $\gamma_{zx}$ , and  $\gamma_{xy}$ , respectively.  $\bar{Q}_{ij}^{(k)}$  can be obtained from the relationships

$$[\bar{Q}]^{(k)} = [T^{-1}]^{(k)}[Q]^{(k)}[T]^{(k)},$$

$$[T]^{(k)} = \begin{bmatrix} m^2 & n^2 & 0 & 0 & 2mn \\ n^2 & m^2 & 0 & 0 & -2mn \\ 0 & 0 & m & -n & 0 \\ 0 & 0 & n & m & 0 \\ -mn & mn & 0 & 0 & m^2 - n^2 \end{bmatrix},$$

where  $[T]^{(k)}$  is the transformation matrix,  $m = \cos\theta_k$ ,  $n = \sin\theta_k$ , and  $\theta_k$  denotes the orientation angle of fibers in laminate axes for a  $k$ th layer.  $Q_{ij}^{(k)}$  can be expressed in terms of engineering constants:

$$Q_{11}^{(k)} = \frac{E_{11}^{(k)}}{1 - \nu_{12}^{(k)}\nu_{21}^{(k)}}, \quad Q_{12}^{(k)} = \frac{\nu_{12}^{(k)}E_{22}^{(k)}}{1 - \nu_{12}^{(k)}\nu_{21}^{(k)}}, \quad Q_{22}^{(k)} = \frac{E_{22}^{(k)}}{1 - \nu_{12}^{(k)}\nu_{21}^{(k)}},$$

$$Q_{66}^{(k)} = G_{12}^{(k)}, \quad Q_{44}^{(k)} = G_{23}^{(k)}, \quad Q_{55}^{(k)} = G_{13}^{(k)}.$$

Other components of the stiffness matrix  $[Q]^{(k)}$  are zero.  $E_{11}^{(k)}$ ,  $E_{22}^{(k)}$ ,  $G_{12}^{(k)}$ ,  $G_{23}^{(k)}$ , and  $G_{13}^{(k)}$  are the longitudinal, transverse, in-plane shear, and out-of-plane stiffnesses of a  $k$ th layer;  $\nu_{12}^{(k)}$  and  $\nu_{21}^{(k)}$  represent the major and minor Poisson's ratios.

The constitutive equations for the laminate can be derived by through-the-thickness integration:

$$\begin{Bmatrix} N_{xx} \\ N_{yy} \\ N_{xy} \\ M_{xx} \\ M_{yy} \\ M_{xy} \end{Bmatrix} = \begin{bmatrix} A_{11} & A_{12} & A_{16} & B_{11} & B_{12} & B_{16} \\ A_{12} & A_{22} & A_{26} & B_{12} & B_{22} & B_{26} \\ A_{16} & A_{26} & A_{66} & B_{16} & B_{26} & B_{66} \\ B_{11} & B_{12} & B_{16} & D_{11} & D_{12} & D_{16} \\ B_{12} & B_{22} & B_{26} & D_{12} & D_{22} & D_{26} \\ B_{16} & B_{26} & B_{66} & D_{16} & D_{26} & D_{66} \end{bmatrix} \begin{Bmatrix} \varepsilon_{xx}^0 \\ \varepsilon_{yy}^0 \\ \gamma_{xy}^0 \\ \kappa_{xx} \\ \kappa_{yy} \\ \kappa_{xy} \end{Bmatrix}, \quad (3a)$$

$$\begin{Bmatrix} Q_y \\ Q_x \end{Bmatrix} = K_s \begin{bmatrix} A_{44} & A_{45} \\ A_{45} & A_{55} \end{bmatrix} \begin{Bmatrix} \gamma_{yz}^0 \\ \gamma_{xz}^0 \end{Bmatrix}, \quad (3b)$$

where  $N_{xx}$ ,  $N_{yy}$ , and  $N_{xy}$  are the membrane normal and shear forces per unit length;  $M_{xx}$ ,  $M_{yy}$ , and  $M_{xy}$  are the bending and twisting moments per unit length;  $Q_x$  and  $Q_y$  are the through-the-thickness shearing forces per unit length.  $A_{ij}$ ,  $B_{ij}$ , and  $D_{ij}$  are expressed as

$$(A_{ij}, B_{ij}, D_{ij}) = \sum_{k=1}^n \int_{z_k}^{z_{k+1}} \bar{Q}_{ij}^{(k)} (1, z, z^2) dz, \quad i, j = 1, 2, 6,$$

$$A_{ij} = \sum_{k=1}^n \int_{z_k}^{z_{k+1}} \bar{Q}_{ij}^{(k)} dz, \quad i, j = 4, 5.$$

The parameter  $K_s$  in (3b) is a shear correction coefficient. The recommended value of the coefficient for a rectangular section is 5/6 [10].

Using the dynamic version of the principle of virtual displacements in association with constitutive equations and strain–displacement relations, the following nonlinear equations of the first-order theory can be obtained [9]:

$$-(N_{xx,x} + N_{xy,x}) + I_0 u_{0,tt} + I_1 \varphi_{x,tt} = 0, \quad (4a)$$

$$-(N_{xy,x} + N_{yy,y}) + I_0 v_{0,tt} + I_1 \varphi_{y,tt} = 0, \quad (4b)$$

$$-(Q_{x,x} + Q_{y,y}) - (N_{xx} w_{0,x} + N_{xy} w_{0,y})_{,x} - (N_{xy} w_{0,x} + N_{yy} w_{0,y})_{,y} - q + I_0 w_{0,tt} = 0, \quad (4c)$$

$$-(M_{xx,x} + M_{xy,y}) + Q_x + I_1 u_{0,tt} + I_2 \varphi_{x,tt} = 0, \quad (4d)$$

$$-(M_{xy,x} + M_{yy,y}) + Q_y + I_1 v_{0,tt} + I_2 \varphi_{y,tt} = 0. \quad (4e)$$

The mass moments of inertia  $I_i$  in Eqs. (4a–4e) are defined as

$$(I_0, I_1, I_2) = \int_{-h/2}^{h/2} (1, z, z^2) \rho_0 dz,$$

where  $h$ ,  $\rho_0$ , and  $q$  are the laminate thickness and density, and the transverse distributed load, respectively.

### 3. Blast Loading

In a blast loading, the pressure increases to a peak overpressure ( $p_{\max}$ ) and then decays to the ambient pressure  $p_0$  in time  $t_0$  (the positive phase); it continues to decay below the ambient pressure and then returns to the pressure once more (the negative phase). When the blast source is far enough from the target, the Friedlander equation [5] can be used to describe the air blast pressure:

$$p(t) = p_{\max} (1 - t/t_0) e^{-\alpha t/t_0},$$

where  $\alpha$  is the waveform parameter. The underwater blast pressure is expressed as [7]

$$p(t) = p_{\max} e^{-t/\lambda}. \quad (5)$$

In an underwater blast wave, no negative phase exists, and  $\lambda$  is a constant. The quantities  $p_{\max}$ ,  $t_0$ ,  $\alpha$ , and  $\lambda$  depend on the explosive type and weight and on the distance between the explosive and target. In addition to the peak overpressure, the impulse should also be taken into the consideration in a blast event, which is defined as the area underneath the pressure–time curve and is the measure of the energy transferred to the target. The impulse controls the level of deflection of the target, and the slope of the impulse–time curve controls the strain rate experienced by the target [11].

### 4. Progressive Damage Model

The progressive damage model introduced by Shokrieh [12] is developed using two-dimensional Hashin-type failure criteria, the rules of sudden degradation of material properties, and empirical relations for the mechanical properties in terms of strain rate.

#### 4.1. Sudden degradation of material properties

The failure modes and the rules of sudden degradation of material properties for a strain-rate-dependent composite can be expressed as follows:

for the tension failure of fiber,

$$\begin{aligned} \text{if } \sigma_{11} > 0, \quad \left( \frac{\sigma_{11}}{X_t} \right)^2 + \left( \frac{\sigma_{12}}{S} \right)^2 &= \begin{cases} \geq 1, & \text{failed} \rightarrow eft = 0, \\ < 1, & \text{elastic} \rightarrow eft = 1, \end{cases} \\ \left[ E_{11}(\dot{\epsilon}_{11}^{(k)}), E_{22}(\dot{\epsilon}_{22}^{(k)}), G_{12}(\dot{\epsilon}_{12}^{(k)}), \nu_{12}, \nu_{21} \right] &\rightarrow [0, 0, 0, 0, 0], \\ \left[ X_t(\dot{\epsilon}_{11}^{(k)}), X_c(\dot{\epsilon}_{11}^{(k)}), Y_t(\dot{\epsilon}_{22}^{(k)}), Y_c(\dot{\epsilon}_{22}^{(k)}), S(\dot{\epsilon}_{12}^{(k)}) \right] &\rightarrow [0, 0, 0, 0, 0]; \end{aligned} \quad (6a)$$

for the compression failure fiber,

$$\begin{aligned} \text{if } \sigma_{11} < 0, \quad \left( \frac{\sigma_{11}}{X_c} \right)^2 &= \begin{cases} \geq 1 & \text{failed} \rightarrow efc = 0, \\ < 1 & \text{elastic} \rightarrow efc = 1, \end{cases} \\ \left[ E_{11}(\dot{\epsilon}_{11}^{(k)}), E_{22}(\dot{\epsilon}_{22}^{(k)}), G_{12}(\dot{\epsilon}_{12}^{(k)}), \nu_{12}, \nu_{21} \right] &\rightarrow [0, 0, 0, 0, 0], \\ \left[ X_t(\dot{\epsilon}_{11}^{(k)}), X_c(\dot{\epsilon}_{11}^{(k)}), Y_t(\dot{\epsilon}_{22}^{(k)}), Y_c(\dot{\epsilon}_{22}^{(k)}), S(\dot{\epsilon}_{12}^{(k)}) \right] &\rightarrow [0, 0, 0, 0, 0]; \end{aligned} \quad (6b)$$

for the fiber-matrix shearing failure,

$$\begin{aligned}
\text{if } \sigma_{11} < 0, \quad \left( \frac{\sigma_{11}}{X_c} \right)^2 + \left( \frac{\sigma_{12}}{S} \right)^2 &= \begin{cases} \geq 1 & \text{failed} \rightarrow efms = 0, \\ < 1 & \text{elastic} \rightarrow efms = 1, \end{cases} \\
\left[ E_{11}(\dot{\varepsilon}_{11}^{(k)}), E_{22}(\dot{\varepsilon}_{22}^{(k)}), G_{12}(\dot{\varepsilon}_{12}^{(k)}), \nu_{12}, \nu_{21} \right] &\rightarrow \\
\rightarrow \left[ E_{11}(\dot{\varepsilon}_{11}^{(k+1)}), E_{22}(\dot{\varepsilon}_{22}^{(k+1)}), 0, 0, 0 \right], & \quad (6c) \\
\left[ X_t(\dot{\varepsilon}_{11}^{(k)}), X_c(\dot{\varepsilon}_{11}^{(k)}), Y_t(\dot{\varepsilon}_{22}^{(k)}), Y_c(\dot{\varepsilon}_{22}^{(k)}), S(\dot{\varepsilon}_{12}^{(k)}) \right] &\rightarrow \\
\rightarrow \left[ X_t(\dot{\varepsilon}_{11}^{(k+1)}), X_c(\dot{\varepsilon}_{11}^{(k+1)}), Y_t(\dot{\varepsilon}_{22}^{(k+1)}), Y_c(\dot{\varepsilon}_{22}^{(k+1)}), 0 \right]; &
\end{aligned}$$

for the tension failure of matrix,

$$\begin{aligned}
\text{if } \sigma_{22} > 0, \quad \left( \frac{\sigma_{22}}{Y_t} \right)^2 + \left( \frac{\sigma_{12}}{S} \right)^2 &= \begin{cases} \geq 1 & \text{failed} \rightarrow emt = 0, \\ < 1 & \text{elastic} \rightarrow emt = 1, \end{cases} \\
\left[ E_{11}(\dot{\varepsilon}_{11}^{(k)}), E_{22}(\dot{\varepsilon}_{22}^{(k)}), G_{12}(\dot{\varepsilon}_{12}^{(k)}), \nu_{12}, \nu_{21} \right] &\rightarrow \\
\rightarrow \left[ E_{11}(\dot{\varepsilon}_{11}^{(k+1)}), 0, G_{12}(\dot{\varepsilon}_{12}^{(k+1)}), \nu_{12}, 0 \right], & \quad (6d) \\
\left[ X_t(\dot{\varepsilon}_{11}^{(k)}), X_c(\dot{\varepsilon}_{11}^{(k)}), Y_t(\dot{\varepsilon}_{22}^{(k)}), Y_c(\dot{\varepsilon}_{22}^{(k)}), S(\dot{\varepsilon}_{12}^{(k)}) \right] &\rightarrow \\
\rightarrow \left[ X_t(\dot{\varepsilon}_{11}^{(k+1)}), X_c(\dot{\varepsilon}_{11}^{(k+1)}), 0, Y_c(\dot{\varepsilon}_{22}^{(k+1)}), S(\dot{\varepsilon}_{12}^{(k+1)}) \right]; &
\end{aligned}$$

for the matrix compression failure:

$$\begin{aligned}
\text{if } \sigma_{22} < 0, \quad \left( \frac{\sigma_{22}}{Y_c} \right)^2 + \left( \frac{\sigma_{12}}{S} \right)^2 &= \begin{cases} \geq 1, & \text{failed} \rightarrow emc = 0, \\ < 1, & \text{elastic} \rightarrow emc = 1, \end{cases} \\
\left[ E_{11}(\dot{\varepsilon}_{11}^{(k)}), E_{22}(\dot{\varepsilon}_{22}^{(k)}), G_{12}(\dot{\varepsilon}_{12}^{(k)}), \nu_{12}, \nu_{21} \right] &\rightarrow \\
\mapsto \left[ E_{11}(\dot{\varepsilon}_{11}^{(k+1)}), 0, G_{12}(\dot{\varepsilon}_{12}^{(k+1)}), \nu_{12}, 0 \right], & \quad (6e) \\
\left[ X_t(\dot{\varepsilon}_{11}^{(k)}), X_c(\dot{\varepsilon}_{11}^{(k)}), Y_t(\dot{\varepsilon}_{22}^{(k)}), Y_c(\dot{\varepsilon}_{22}^{(k)}), S(\dot{\varepsilon}_{12}^{(k)}) \right] &\rightarrow \\
\rightarrow \left[ X_t(\dot{\varepsilon}_{11}^{(k+1)}), X_c(\dot{\varepsilon}_{11}^{(k+1)}), Y_t(\dot{\varepsilon}_{22}^{(k+1)}), 0, S(\dot{\varepsilon}_{12}^{(k+1)}) \right], &
\end{aligned}$$

where  $\sigma_{11}$  is the stress in the fiber direction,  $\sigma_{22}$  is the stress in the direction transverse to the fiber, and  $\sigma_{12}$  is the in-plane shear stress.  $X_t$ ,  $X_c$ ,  $Y_t$ ,  $Y_c$ , and  $S$  are the longitudinal tensile strength, the longitudinal compressive strength, the transverse tensile strength, the transverse compressive strength, and the in-plane shear strength, respectively;  $eft$ ,  $efc$ ,  $efms$ ,  $emt$ , and  $emc$  denote the damage variables in fiber tension, fiber compression, fiber-matrix shearing, matrix tension, and matrix compression failure modes, respectively. In addition,  $\dot{\varepsilon}_{11}^{(k)}$ ,  $\dot{\varepsilon}_{22}^{(k)}$ , and  $\dot{\varepsilon}_{12}^{(k)}$  are the rates of longitudinal, transverse, and shear strains at a  $k$ th time step, respectively;  $\sigma_{11}$ ,  $\sigma_{22}$ , and  $\sigma_{12}$  for an  $n$ th layer are calculated from the relationship

$$\begin{Bmatrix} \sigma_{11} \\ \sigma_{22} \\ \sigma_{12} \end{Bmatrix}^{(n)} = \begin{bmatrix} m^2 & n^2 & -2mn \\ n^2 & m^2 & 2mn \\ -mn & mn & m^2 - n^2 \end{bmatrix}^{(n)} \begin{Bmatrix} \sigma_{xx} \\ \sigma_{yy} \\ \sigma_{xy} \end{Bmatrix}^{(n)}.$$

TABLE 1. Material Constants in the Regression Function of the Mechanical Properties of Glass/Epoxy Composites [13-15]

Constant	Stiffness, GPa			Strength, MPa				
	$E_{11}$	$E_{22}$	$G_{12}$	$X_t$	$X_c$	$Y_t$	$Y_c$	$S$
$\alpha$	37.243	10.037	4.919	788.120	243.497	43.451	109.970	31.316
$\beta$	1.139	0.437	-0.941	7.721	316.151	13.088	0.110	15.656
$\gamma$	0.276	0.262	0.054	0.886	0.0874	0.131	1.278	0.086

#### 4.2. Mechanical property–strain rate relations

The mechanical properties of a composite are functions of strain rate. When a composite plate is exposed to a dynamic loading, different points of the plate are subjected to different time-dependent strain rates, and therefore they have different mechanical properties. Shokrieh and Omid [13-15] investigated the effect of strain rate on the mechanical properties of uni-directional glass/epoxy composites by using a servohydraulic apparatus at varying strain rates, ranging from 0.001 to 100 1/s. In their study, the mechanical properties are plotted versus the logarithms of strain rate, and the data are fitted by using the regression function

$$M(\dot{\varepsilon}) = \alpha + \beta \dot{\varepsilon}^\gamma, \quad (7)$$

where  $M$  and  $\dot{\varepsilon}$  are the mechanical property and strain rate, respectively;  $\alpha$ ,  $\beta$ , and  $\gamma$  are material constants. Table 1 shows the values of  $\alpha$ ,  $\beta$ , and  $\gamma$  for various mechanical properties of glass/epoxy composites.

#### 5. Finite-Difference Model

Inserting Eqs. (3a) and (3b) into Eqs. (4a)-(4e) and using Eq. (1), the equations of motion can be expressed in terms of the displacements  $u_0, v_0, w_0, \varphi_x$ , and  $\varphi_y$ . The nonlinear coupled partial differential equations can be reduced to a set of ordinary differential equations in the time domain by using the finite-difference approximation for the displacement field. Employing the central finite-difference approximations, the differential equations, initial conditions, and boundary conditions can be converted into finite-difference expressions at a mesh point  $(i, j)$ . The central finite-difference equations for the first- and second-order derivatives of an arbitrary variable  $f$  can be written as

$$\begin{aligned} f_{,x} &= \frac{1}{2h}(-f_{-1+i,j} + f_{1+i,j}), \\ f_{,y} &= \frac{1}{2h}(-f_{i,-1+j} + f_{i,1+j}), \\ f_{,xx} &= \frac{1}{h^2}(f_{-1+i,j} - 2f_{i,j} + f_{1+i,j}), \\ f_{,xy} &= \frac{1}{4h^2}(f_{-1+i,-1+j} - f_{-1+i,1+j} - f_{1+i,-1+j} + f_{1+i,1+j}), \\ f_{,yy} &= \frac{1}{h^2}(f_{i,-1+j} - 2f_{i,j} + f_{i,1+j}), \end{aligned} \quad (8)$$

where  $f_{i,j}$  and  $h$  denote the value of  $f$  at the mesh point  $(i, j)$  and the spatial length scale, respectively. The finite-difference form of Eq. (4a) is given in Appendix A. Equations (4b)-(4e) can be similarly converted into finite-difference expressions by using Eqs. (7).

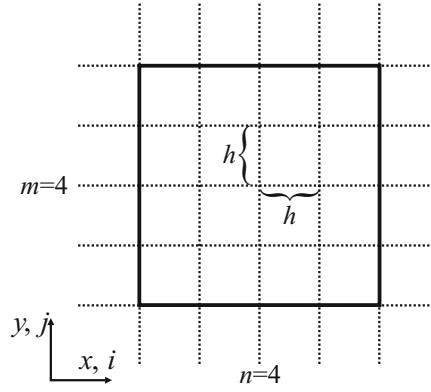


Fig. 2. Finite-difference mesh.

Figure 2 shows an example of the finite-difference mesh. For each mesh point, five ordinary differential equations in the time domain are obtained. After assembling these equations for all mesh points, the matrix form of the equations can be written as

$$\mathbf{M}\ddot{\mathbf{U}} = \mathbf{F}_{\text{ext}}(t) - \mathbf{F}_{\text{int}}(\mathbf{U}), \quad (9)$$

where  $\mathbf{M}$ ,  $\mathbf{F}_{\text{ext}}$ , and  $\mathbf{F}_{\text{int}}$  are the mass matrix and the external and internal force vectors, respectively.  $\mathbf{U}$  and  $\ddot{\mathbf{U}}$  are the displacement and acceleration vectors, respectively. The displacement vector can be written as

$$\mathbf{U} = \{\mathbf{u}_{i,j}, \mathbf{v}_{i,j}, \mathbf{w}_{i,j}, \varphi_x^{i,j}, \varphi_y^{i,j}\}^T, \quad i = 1, 2, \dots, n-1, j = 1, 2, \dots, m-1.$$

As shown in Fig. 2,  $n$  and  $m$  represent the numbers of division in the  $x$  and  $y$  directions, respectively. In order to reduce the set of ordinary differential equations (9) to algebraic ones, the time derivatives are approximated using the Newmark implicit time integration scheme [9]. At the time  $t + \Delta t$ , equation (9) can be rewritten as

$$\mathbf{M}\ddot{\mathbf{U}}^{(t+\Delta t)} + \mathbf{K}^{(t)}\Delta\mathbf{U} = \mathbf{F}_{\text{ext}}^{(t+\Delta t)}(t) - \mathbf{F}_{\text{int}}^{(t)}(\mathbf{U}),$$

where  $\mathbf{K}$  is the tangential stiffness matrix, which is defined as

$$\mathbf{K} = \frac{\partial \mathbf{F}_{\text{int}}}{\partial \mathbf{U}}. \quad (10)$$

The solution procedure is as follows

Step 1: calculate  $a_1 = \alpha\Delta t$ ,  $a_2 = (1 - \alpha)\Delta t$ ,  $a_3 = 1 / (\beta\Delta t^2)$ ,  $a_4 = a_3\Delta t$ ,  $a_5 = 1 / (2\beta) - 1$ ;

Step 2: initialize  $\mathbf{U}^{(0)}$ ,  $\dot{\mathbf{U}}^{(0)}$ , and  $\ddot{\mathbf{U}}^{(0)}$

Step 3: calculate  ${}^{(0)}\widehat{\mathbf{K}} = \mathbf{K}^{(t)} + a_0\mathbf{M}$  and  $\widehat{\mathbf{F}} = {}^{(0)}\mathbf{F}_{\text{ext}}^{(t+\Delta t)} + \mathbf{M}(a_1\dot{\mathbf{U}}^{(t)} + a_2\ddot{\mathbf{U}}^{(t)}) - \mathbf{F}_{\text{int}}^{(t)}$ ;

Step 4: solve  ${}^{(0)}\widehat{\mathbf{K}}\Delta\mathbf{U} = {}^{(0)}\widehat{\mathbf{F}}$  and calculate  ${}^{(1)}\mathbf{F}_{\text{int}}^{(t+\Delta t)}$ ;

Step 5: set iteration  $i = 2$

Step 6: update  ${}^{(i-1)}\mathbf{K}^{(t+\Delta t)}$  using (10)

Step 7: calculate

$${}^{(i-1)}\ddot{\mathbf{U}}^{(t+\Delta t)} = a_0{}^{(i-1)}\Delta\mathbf{U} - a_1\dot{\mathbf{U}}^{(t)} - a_2\ddot{\mathbf{U}}^{(t)}, \quad {}^{(i-1)}\widehat{\mathbf{K}} = {}^{(i-1)}\mathbf{K}^{(t+\Delta t)} + a_0\mathbf{M}, \text{ and}$$

$${}^{(i-1)}\mathbf{R} = \mathbf{F}_{\text{ext}}^{(t+\Delta t)} - \mathbf{M}{}^{(i-1)}\mathbf{U}^{(t+\Delta t)} - {}^{(i-1)}\mathbf{F}_{\text{int}}^{(t+\Delta t)};$$

Step 8: solve  ${}^{(i-1)}\widehat{\mathbf{K}}d\mathbf{U} = {}^{(i-1)}\mathbf{R}$  and update  ${}^{(i)}\Delta\mathbf{U} = {}^{(i-1)}\Delta\mathbf{U} + {}^{(i)}d\mathbf{U}$ ;

Step 9: update  ${}^{(i)}\mathbf{F}_{\text{int}}^{(t+\Delta t)}$ ;



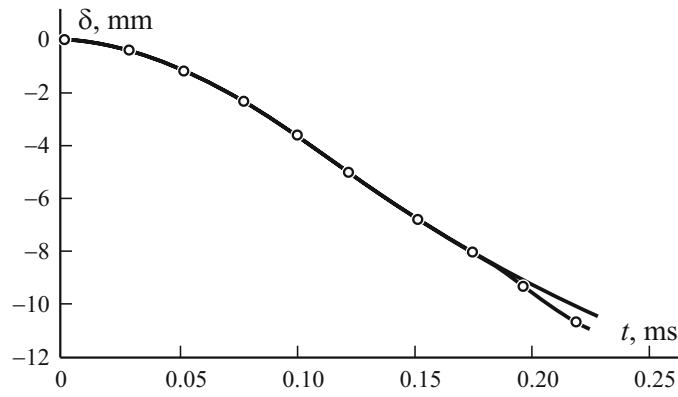


Fig. 3. Comparison of deflections  $\delta$  at the center of the plate: (—) — present; (—○—) — data from [7].

Step 10: check convergence:

if yes, go to step 11, if no, set  $i = i + 1$  and go to step 6;

Step 11: calculate acceleration, velocity and displacement vectors:

$$\ddot{\mathbf{U}}^{(t+\Delta t)} = a_0 \Delta \mathbf{U} - a_1 \dot{\mathbf{U}}^{(t)} - a_2 \ddot{\mathbf{U}}^{(t)}, \quad \dot{\mathbf{U}}^{(t+\Delta t)} = \dot{\mathbf{U}}^{(t)} + a_3 \ddot{\mathbf{U}}^{(t)} + a_4 \ddot{\mathbf{U}}^{(t+\Delta t)}, \text{ and}$$

$$\mathbf{U}^{(t+\Delta t)} = \mathbf{U}^{(t)} + \Delta \mathbf{U};$$

Step 12: calculate the strain and stress tensors using Eqs. (1) and (2), respectively;

Step 13: calculate the strain rate  $\dot{\boldsymbol{\epsilon}}^{(t+\Delta t)} = \frac{1}{\Delta t} (\boldsymbol{\epsilon}^{(t+\Delta t)} - \boldsymbol{\epsilon}^{(t)})$ ;

Step 14: check for the failure in layers using Eqs. (6):

if failed, use the rules of sudden material property degradation and go to 14, if not, go to step 15

Step 15: update material properties using Eq. (7);

Step 16: go to the next time step.

Here,  $\Delta t$  is the time step,  $i$  denotes the iteration, and  $\alpha$  and  $\beta$  determine the stability and accuracy of the scheme.

In the present work, the constant-average acceleration method with  $\alpha = \beta = 0.5$  is used.

## 6. Verification Study

In order to validate the present model, a comparison with the results obtained by Batra and Hassan [7] was carried out. In [7], the response of a composite panel exposed to an underwater explosive load is obtained using the three-dimensional finite-element method. A 10-mm-thick, 220×220-mm square AS4/PEEK composite panel with a fiber volume content of 0.6 was used. The mechanical properties were:

$E_1 = 130.86$  GPa,  $E_2 = 14.7$  GPa,  $G_{12} = G_{23} = 5.44$  GPa,  $X_t = 1375$  MPa,  $X_c = 1080$  MPa,  $Y_t = 78$  MPa,  $Y_c = 150$  MPa,  $S = 70$  MPa,  $\rho = 1640$  kg/m<sup>3</sup>, and  $\nu_{12} = 0.3$ .

The plate was made of four plies with fiber orientation  $\theta = 0^\circ$ , clamped along all four edges, and subjected to a non-uniform blast pressure from 64 kg of TNT with a standoff distance of 10 m. The pressure distribution over the plate was:

$$p(r,t) = (-0.0005r^4 + 0.01r^3 - 0.0586r^2 - 0.001r + 1)p(t),$$

where  $r$  is the distance from the center of the plate in cm, and  $p(t)$  denotes the pressure at the center of the plate, which can be expressed by Eq. (5) with  $p_{\max} = 17.68$  MPa and  $\lambda = 0.424$ . The strain rate effects on the transverse and shear stiffnesses are considered in [7], but due to the lack of information in [7], all material properties were assumed to be constant in the

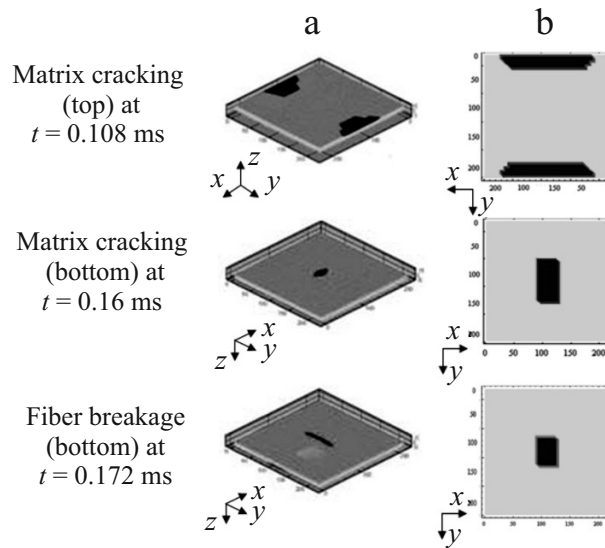


Fig. 4. Comparison of predicted failure modes: (a) [7] and (b) present model.

verification study. Figure 3 depicts a comparison between the deflection  $\delta$  at the center of the plate reported in [7] and that obtained from the present model. The failure modes given by the present model and in [7] are also shown in Fig. 4. A good agreement can be observed between the results.

## 7. Numerical Results and Discussion

A 16-mm-thick, 200×200-mm glass/epoxy composite plate with a  $[0]_s$  ply stacking was considered. The fiber volume fraction of the composite was 50%. The plate was clamped at all edges and subjected to a uniform underwater blast load. The parameters of the load (Eq. (5)) from 51 kg of TNT with a standoff distance of 15 m are  $p_{\max} = 10$  MPa and  $\lambda = 0.4$ .

In order to investigate the strain rate effects two material models were considered.

Static model. The mechanical properties were obtained from static tests and were constant (see Table 1):

$E_{11} = 37.243$  GPa,  $E_{22} = 10.037$  GPa,  $G_{12} = G_{23} = 4.919$  GPa,  $X_t = 788.122$  MPa,  $X_c = 243.497$  MPa,  $Y_t = 43.451$  MPa,  $Y_c = 109.97$  MPa, and  $S = 31.316$  MPa.

Dynamic model. The mechanical properties were strain-rate-dependent and were recalculated from Eq. (7).

The density and Poisson's ratio did not vary with strain rate:

$\rho = 2100$  kg/m<sup>3</sup>, and  $\nu_{12} = 0.237$ .

From convergence studies, it was found that 400 mesh points and a time increment of 0.012 ms were adequate for the numerical simulation.

### 7.1. Effect of strain rate

Figure 5 depicts the time histories of deflection at the center of a plate with a  $[0]_s$  ply stacking sequence. Results of the static and dynamic models are shown by dashed and solid curves, respectively. As seen, the maximum deflection at the center (absolute value) obtained from the static model is larger than that given by the dynamic one. This is due to the fact that, the stiffness in the dynamic model increases with strain rate, and therefore the static model, which has constant mechanical properties, is softer than the dynamic one. This result is consistent with that obtained by Zhu et al. [8].

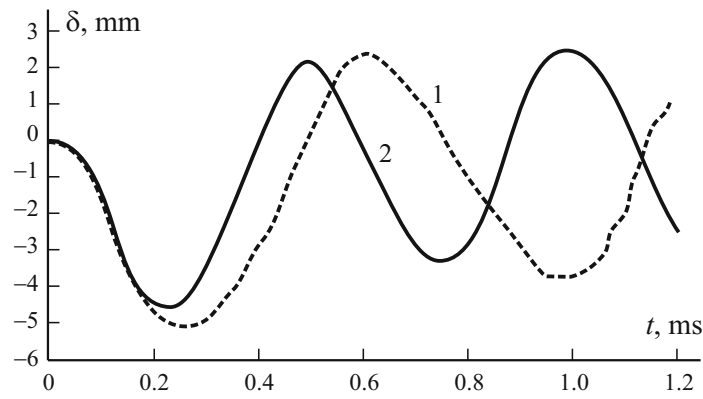


Fig. 5. Deflection at the center of the plate for the static (1) and dynamic (2) models.

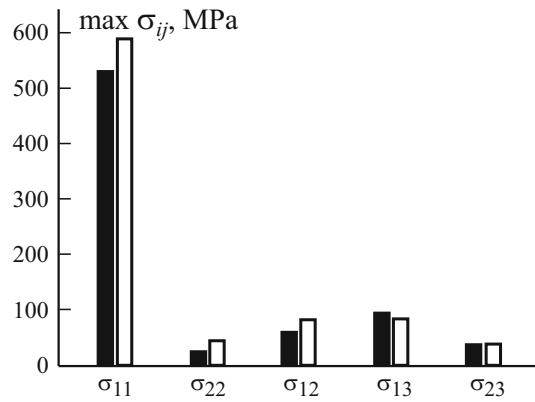


Fig. 6. Maximum stresses for the static ( $\square$ ) and dynamic ( $\blacksquare$ ) models.

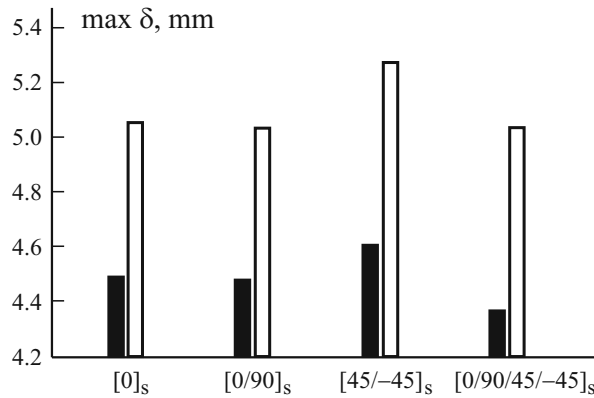


Fig. 7. Maximum deflection at the center for various stacking sequences: for static ( $\square$ ) and dynamic ( $\blacksquare$ ) models.

Figure 6 shows the maximum stresses for the static and dynamic models during the loading. It can be observed that the stresses obtained from the static model are higher than those given by the dynamic one (except for  $\sigma_{13}$ ). This can be explained by the fact that the maximum deflection at the center for the static model is greater than for the dynamic one, which leads to greater strains and stresses for the static model. As shown in Fig. 6, the maximum out-of-plane shear stress calculated from the dynamic model is slightly higher than that found from the static one. However, the mean value of  $\sigma_{13}$  during the loading is 20 MPa for the static model and only 15.6 MPa for the dynamic one.

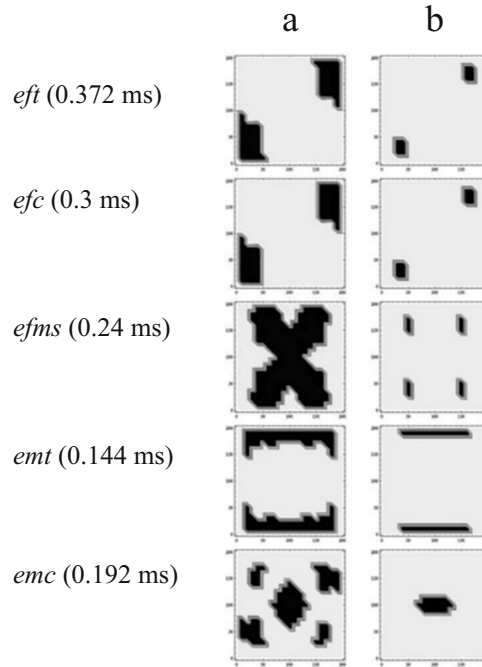


Fig. 8. Comparison of failure modes for the static (a) and dynamic (b) models.

## 7.2. Effect of stacking sequence

To investigate the effect of stacking sequence on the dynamic response of a composite plate under a blast load, 200×200×16-mm glass/epoxy composite clamped plates with  $[0]_s$ ,  $[0/90]_s$ ,  $[+45/-45]_s$ , and  $[0/90/+45/-45]_s$  layups were analyzed. The maximum deflections  $w_{\max}$  at the center of the plates are given in Fig. 7. As seen, the trends for the static and dynamic models are the same. It can be observed that, for both the models, the maximum deflection at the center of the  $[+45/-45]_s$  plate is larger than that of the other ones. This is due to the higher flexibility of the  $[+45/-45]_s$  stacking sequence in comparison with those of the other stacking sequences.

## 7.3. Effect of strain rate on failure modes

Figure 8 exhibits fringe plots of various damage variables at the top surface of a 200×200×16-mm clamped glass/epoxy composite plate with the  $[0]_s$  stacking sequence under a uniform underwater blast load with  $\lambda = 0.4$  and  $p_{\max} = 10$  MPa. It can be concluded from these plots that, for all failure modes, at a specific time, the failed region obtained using the static model is larger than that given by the dynamic model. This is due to the fact that the strength of the dynamic model increases with strain rate and is higher than that of the static one. It can also be observed that, for a specific failure mode, the location of damage initiation for the static and dynamic models are similar.

The propagation of cracks in interfaces, which is known as the delamination failure mode, depends on the transverse normal ( $\sigma_{33}$ ) and transverse shear stresses ( $\sigma_{13}$ , and  $\sigma_{23}$ ). According to the 3-D Hashin-type criteria, the delamination failure mode can be predicted using the relations [12]

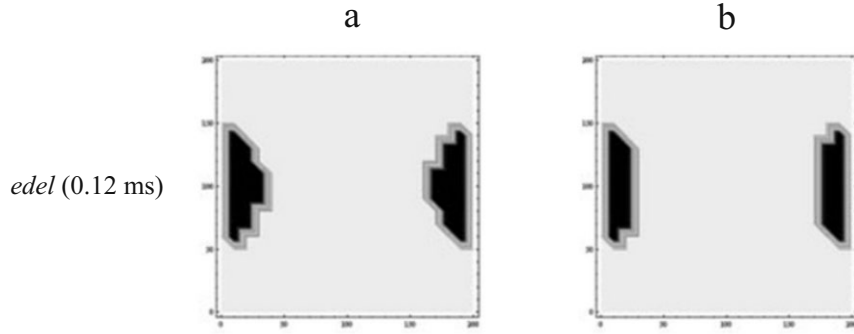


Fig. 9. Delamination failure mode for the static (a) and dynamic (b) models.

$$\begin{aligned}
 \text{if } \sigma_{33} \geq 0, & \Rightarrow \left( \frac{\sigma_{33}}{Z_t} \right)^2 + \left( \frac{\sigma_{13}}{S_{13}} \right)^2 + \left( \frac{\sigma_{23}}{S_{23}} \right)^2 = \begin{cases} \geq 1, & \text{failed} \\ < 1, & \text{elastic} \end{cases} \\
 \text{if } \sigma_{33} < 0, & \Rightarrow \left( \frac{\sigma_{33}}{Z_c} \right)^2 + \left( \frac{\sigma_{13}}{S_{13}} \right)^2 + \left( \frac{\sigma_{23}}{S_{23}} \right)^2 = \begin{cases} \geq 1, & \text{failed,} \\ < 1, & \text{elastic,} \end{cases}
 \end{aligned} \tag{11}$$

where  $Z_t$  and  $Z_c$  denote the normal tensile and compressive strengths, respectively.  $S_{13}$  and  $S_{23}$  represent the out-of-plane shear strengths. As mentioned before, based on the first-order theory, the transverse normal stress is zero. Therefore, Eq. (11) is reduced to

$$\left( \frac{\sigma_{13}}{S_{13}} \right)^2 + \left( \frac{\sigma_{23}}{S_{23}} \right)^2 = \begin{cases} \geq 1, & \text{failed} \rightarrow edel = 0, \\ < 1, & \text{elastic} \rightarrow edel = 1, \end{cases}$$

where,  $edel$  is the damage variable for the delamination failure mode. In Fig. 9, at  $S_{13} = S_{23} = S = 31.316$  MPa, the delamination failure mode at the bottom surface according to the static and dynamic material models is shown. As seen, in both the cases, the delamination occurs at the edges perpendicular to the fiber direction. Similar fringe plots were also obtained for the top surface. Since variations in the out-of-plane strength and stiffness with strain rate were unknown, these characteristics were assumed to be constant.

Although a 2-D model was used for modeling of the delamination, this failure mode is a three-dimensional phenomenon. A proper modeling of delamination can be carried out using 3-D theories and approaches for composite plates.

## Conclusions

In the present study, nonlinear equations of motion for a laminated composite plate under blast loading based on the first-order shear deformation theory (FSDT) are derived. The rules of material property degradation in association with Hashin-type failure criteria are used to model various failure modes. The equations derived are solved numerically using the finite-difference method. The validity of the model is examined by quantitative and qualitative comparisons of calculation results with those presented in the literature. The rate effects are taken into account by using rate-dependent material properties. The following conclusions can be drawn from the present work.

- The maximum deflection at the center of the plate considered and the maximum stresses obtained using the static model (with constant material properties) are higher than those obtained using the dynamic model (with strain-rate dependent material properties).

- The influence of stacking sequence on the maximum deflection at the center of the plate obtained using the static and dynamic models is similar; the largest maximum deflection is obtained for composite plate with the [+45/-45]<sub>s</sub> stacking sequence.
- At a certain time, for all failure modes, the failed regions found using the static model are larger than those obtained using the dynamic model. However, in a specific failure mode, the location of damage initiation is the same for both the models.

## REFERENCES

1. J. N. Reddy, "Geometrically nonlinear transient analysis of laminated composite panels," *Amer. Inst. of Aeronautics and Astronautics J.*, **21**, 621-629 (1983).
2. L. Librescu and A. Nosier, "Response of laminated composite flat panels to sonic boom and explosive blast loadings," *AIAA J.*, **28**, No. 2, 345-352 (1990).
3. H. S. Turkmen and Z. Mecitoglu, "Dynamic response of a stiffened laminated composite plate subjected to blast load," *J. of Sound and Vibration*, **221**, No. 3, 371-389 (1999).
4. H. S. Turkmen, "Structural response of laminated composite shells subjected to blast loading: comparison of experimental and theoretical methods," *J. of Sound and Vibration*, **249**, No. 4, 663-678 (2002).
5. Z. Kazanci and Z. Mecitoglu, "Nonlinear dynamic behavior of simply supported laminated composite plates subjected to blast load," *J. of Sound and Vibration*, **317**, 883-897 (2008).
6. J. Chen, D. Dawe, and S. Wang, "Nonlinear transient analysis of rectangular composite laminated plates," *Compos. Struct.*, **49**, 129-139 (2000).
7. R. C. Batra and N. M. Hassan, "Response of fiber reinforced composites to underwater explosive loads," *Composites: Part B*, **38**, 448-468 (2007).
8. L. Zhu, A. Chattopadhyay, and R. K. Goldberg, "Nonlinear transient response of strain rate dependent using multiscale simulation", *Int. J. of Solids and Structures*, **43**, 2602-2630 (2006).
9. J. N. Reddy, *Mechanics of Laminated Composite Plates and Shells (Theory and Analysis)*, CRC Press-USA (2004).
10. Livermore Software Technology Corporation, *LS-DYNA 971 keyword user's manual*, California-USA (2006).
11. A. Wright and M. French, "The response of carbon fibre composites to blast loading via the Europa CAFV program," *J. of Mater. Sci.*, **43**, No. **20**, 6619-6629 (2008).
12. M. M. Shokrieh, *Progressive Fatigue Damage Modeling of Composite Materials*, Ph.D. thesis, Department of Mechanical Engineering, McGill University Montreal-Canada (1996).
13. M. M. Shokrieh and M. J. Omid, "Tension behavior of unidirectional glass/epoxy composites under different strain rates," *Compos. Struct.*, **88**, No. 4, 595-601 (2009).
14. M. M. Shokrieh and M. J. Omid, "Compressive response of glass-fiber reinforced polymeric composites to increasing compressive strain rates," *Compos. Struct.*, **89**, No. 4, 517-523 (2009).
15. M. M. Shokrieh and M. J. Omid, "Investigation of strain rate effects on in-plane shear properties of glass/epoxy composites," *Compos. Struct.*, **91**, No. 1, 95-102 (2009).

## Appendix A

In order to convert Eq. (4a) into a finite difference form,  $N_{xx}$  and  $N_{xy}$  are written in terms of displacements and rotations by using Eqs. (3a), (3b) and (1) for a mesh point  $(i, j)$ :

$$N_{xx}^{i,j} = A_{11}^{i,j} \left[ u_{,x}^{i,j} + \frac{1}{2} (w_{,x}^{i,j})^2 \right] + A_{12}^{i,j} \left[ v_{,y}^{i,j} + \frac{1}{2} (w_{,y}^{i,j})^2 \right] + A_{13}^{i,j} \left( u_{,y}^{i,j} + v_{,x}^{i,j} + w_{,x}^{i,j} w_{,y}^{i,j} \right) + B_{11}^{i,j} \varphi_{x,x}^{i,j} + B_{12}^{i,j} \varphi_{y,y}^{i,j} + B_{13}^{i,j} \left( \varphi_{x,y}^{i,j} + \varphi_{y,x}^{i,j} \right),$$

$$N_{xy}^{i,j} = A_{13}^{i,j} \left[ u_{,x}^{i,j} + \frac{1}{2} (w_{,x}^{i,j})^2 \right] + A_{23}^{i,j} \left[ v_{,y}^{i,j} + \frac{1}{2} (w_{,y}^{i,j})^2 \right] \\ + A_{33}^{i,j} \left( u_{,y}^{i,j} + v_{,x}^{i,j} + w_{,x}^{i,j} w_{,y}^{i,j} \right) + B_{13}^{i,j} \varphi_{x,x}^{i,j} + B_{23}^{i,j} \varphi_{y,y}^{i,j} + B_{33}^{i,j} \left( \varphi_{x,y}^{i,j} + \varphi_{y,x}^{i,j} \right).$$

The derivatives of  $N_{xx}$  and  $N_{xy}$  with respect to  $x$  can be obtained as

$$N_{xx,x}^{i,j} = A_{11}^{i,j} \left( u_{,xx}^{i,j} + w_{,x}^{i,j} w_{,xx}^{i,j} \right) + A_{12}^{i,j} \left( v_{,yx}^{i,j} + w_{,y}^{i,j} w_{,yx}^{i,j} \right) \\ + A_{13}^{i,j} \left( u_{,yx}^{i,j} + v_{,xx}^{i,j} + w_{,xx}^{i,j} w_{,y}^{i,j} + w_{,x}^{i,j} w_{,yx}^{i,j} \right) + B_{11}^{i,j} \varphi_{x,xx}^{i,j} + B_{12}^{i,j} \varphi_{y,yx}^{i,j} + B_{13}^{i,j} \left( \varphi_{x,yx}^{i,j} + \varphi_{y,xx}^{i,j} \right), \quad (\text{A.1})$$

$$N_{xy,y}^{i,j} = A_{13}^{i,j} \left( u_{,xy}^{i,j} + w_{,x}^{i,j} w_{,xy}^{i,j} \right) + A_{23}^{i,j} \left( v_{,yy}^{i,j} + w_{,y}^{i,j} w_{,yy}^{i,j} \right) \\ + A_{33}^{i,j} \left( u_{,yy}^{i,j} + v_{,xy}^{i,j} + w_{,xy}^{i,j} w_{,y}^{i,j} + w_{,x}^{i,j} w_{,yy}^{i,j} \right) + B_{13}^{i,j} \varphi_{x,xy}^{i,j} + B_{23}^{i,j} \varphi_{y,yy}^{i,j} + B_{33}^{i,j} \left( \varphi_{x,yy}^{i,j} + \varphi_{y,xy}^{i,j} \right). \quad (\text{A.2})$$

Finding the finite-difference form of derivatives of displacements and rotations by using Eqs. (8) and inserting the finite-difference expressions in (A.1) and (A.2), one can obtain the finite-difference form of Eq. (4a):

$$-\frac{1}{8h^3} \left\{ 4A_{23}^{i,j} \left[ 2h(v_{i,-1+j} - 2v_{i,j} + v_{i,1+j}) + (-w_{i,-1+j} + w_{i,1+j})(w_{i,-1+j} - 2w_{i,j} + w_{i,1+j}) \right] \right. \\ + 4A_{11}^{i,j} \left[ 2h(u_{-1+i,j} - 2u_{i,j} + u_{1+i,j}) + (-w_{-1+i,j} + w_{1+i,j})(w_{-1+i,j} - 2w_{i,j} + w_{1+i,j}) \right] \\ + A_{12}^{i,j} \left[ 2h(v_{-1+i,-1+j} - v_{-1+i,1+j} - v_{1+i,-1+j} + v_{1+i,1+j}) \right. \\ \left. + (-w_{i,-1+j} + w_{i,1+j})(w_{-1+i,-1+j} - w_{-1+i,1+j} - w_{1+i,-1+j} + w_{1+i,1+j}) \right] \\ + A_{33}^{i,j} \left[ 8h(u_{i,-1+j} - 2u_{i,j} + u_{i,1+j}) + 2h(v_{-1+i,-1+j} - v_{-1+i,1+j} - v_{1+i,-1+j} + v_{1+i,1+j}) \right. \\ \left. + 4(w_{i,-1+j} - 2w_{i,j} + w_{i,1+j})(-w_{-1+i,j} + w_{1+i,j}) \right. \\ \left. + (-w_{i,-1+j} + w_{i,1+j})(w_{-1+i,-1+j} - w_{-1+i,1+j} - w_{1+i,-1+j} + w_{1+i,1+j}) \right] \\ + A_{13}^{i,j} \left[ 2h(u_{-1+i,-1+j} - u_{-1+i,1+j} - u_{1+i,-1+j} + u_{1+i,1+j}) \right. \\ \left. + (-w_{-1+i,j} + w_{1+i,j})(w_{-1+i,-1+j} - w_{-1+i,1+j} - w_{1+i,-1+j} + w_{1+i,1+j}) \right] \\ + A_{13}^{i,j} \left[ 2h(u_{-1+i,-1+j} - u_{-1+i,1+j} - u_{1+i,-1+j} + u_{1+i,1+j}) + 8h(v_{-1+i,j} - 2v_{i,j} + v_{1+i,j}) \right. \\ \left. + 4(-w_{i,-1+j} + w_{i,1+j})(w_{-1+i,j} - 2w_{i,j} + w_{1+i,j}) \right. \\ \left. + (-w_{-1+i,j} + w_{1+i,j})(w_{-1+i,-1+j} - w_{-1+i,1+j} + w_{i,1+j})(w_{-1+i,j} - 2w_{i,j} + w_{1+i,j}) \right. \\ \left. + (-w_{-1+i,j} + w_{1+i,j})(w_{-1+i,-1+j} - w_{-1+i,1+j} - w_{1+i,-1+j} + w_{1+i,1+j}) \right] \\ + 8hB_{11}^{i,j} \left( \varphi_x^{-1+i,j} - 2\varphi_x^{i,j} + \varphi_x^{1+i,j} \right) + 2hB_{13}^{i,j} \left( \varphi_x^{-1+i,-1+j} - \varphi_x^{-1+i,1+j} - \varphi_x^{1+i,-1+j} + \varphi_x^{1+i,1+j} \right) \\ \left. + 8hB_{23}^{i,j} \left( \varphi_y^{i,-1+j} - 2\varphi_y^{i,j} + \varphi_y^{i,1+j} \right) \right\}$$

$$\begin{aligned}
& +2hB_{13}^{i,j} \left( \varphi_x^{-1+i,-1+j} - \varphi_x^{-1+i,1+j} - \varphi_x^{1+i,-1+j} + \varphi_x^{1+i,1+j} + 4\varphi_y^{-1+i,j} - 8\varphi_y^{i,j} + 4\varphi_y^{1+i,j} \right) \\
& +2hB_{12}^{i,j} \left( \varphi_y^{-1+i,-1+j} - \varphi_y^{-1+i,1+j} - \varphi_y^{1+i,-1+j} + \varphi_y^{1+i,1+j} \right) + 2hB_{33}^{i,j} \left( 4\varphi_x^{i,-1+j} - 8\varphi_x^{i,j} \right. \\
& \left. + 4\varphi_x^{i,1+j} + \varphi_y^{-1+i,-1+j} - \varphi_x^{-1+i,1+j} - \varphi_x^{1+i,-1+j} + \varphi_x^{1+i,1+j} \right) \Big\} + I_0 \ddot{u}_{i,j} + I_1 \ddot{\varphi}_x^{i,j} = 0.
\end{aligned}$$